Supporting Information for: Enhanced Electromechanical Response due to Inhomogeneous Strain in Monolayer MoS$_2$

Claire M. Ganski[†,‡], Alex C. De Palma[†,‡], Edward T. Yu*[†,‡,§]

[†]Microelectronics Research Center, University of Texas at Austin, Austin, Texas 78758, United States; [‡]Texas Materials Institute, University of Texas at Austin, Austin, Texas 78712, United States; [§]Department of Electrical and Computer Engineering, University of Texas at Austin, Austin, Texas 78712, United States

*Corresponding Author: Edward T. Yu - Email: ety@ece.utexas.edu

Supporting Note 1*: MoS$_2$ monolayer identification*

Determining the number of layers in a 2D material sample is best achieved using a combination of methods, as AFM step-heights on their own can be unreliable on the nanometer scale[1,2]. After mechanically exfoliating MoS$_2$ onto PDMS, we first locate potential monolayers based on their low contrast under an optical microscope [Figure S1a]. Next, photoluminescence (PL) and Raman spectroscopy are performed on the selected areas. Due to their direct bandgaps, monolayers of MoS$_2$ are expected to produce high PL intensities compared to bilayers or thicker samples. Monolayer MoS$_2$ is further distinguished by a separation of approximately 20 cm^{-1} between its A$_{1g}$ and E$_{2g}^1$ Raman modes[3–5].

Figures S1e-f show the PL and Raman spectra of neighboring monolayer, bilayer, and trilayer regions in a flake of exfoliated MoS$_2$. A clear pattern is exhibited in which the PL intensity decreases and the Raman peak separation increases from monolayer to bilayer and from bilayer to trilayer. Figures S1a-d characterize the MoS$_2$ flake shown in Figures 5 and 6 of the main text,

1   which resides on the same exfoliated sample as the flake in Figures S1e-f. The AFM step-height

2   in Figure S1b (corresponding to the white arrow in Figure S1a) is measured as 0.85 nm, which

3   slightly exceeds the known MoS_2 layer thickness of 0.65 nm. However, the PL intensity and Raman

4   peak separation of this area are consistent with the results for monolayers in Figures S1e-f and in

5   previous works, confirming that it is in fact a single layer of MoS_2.
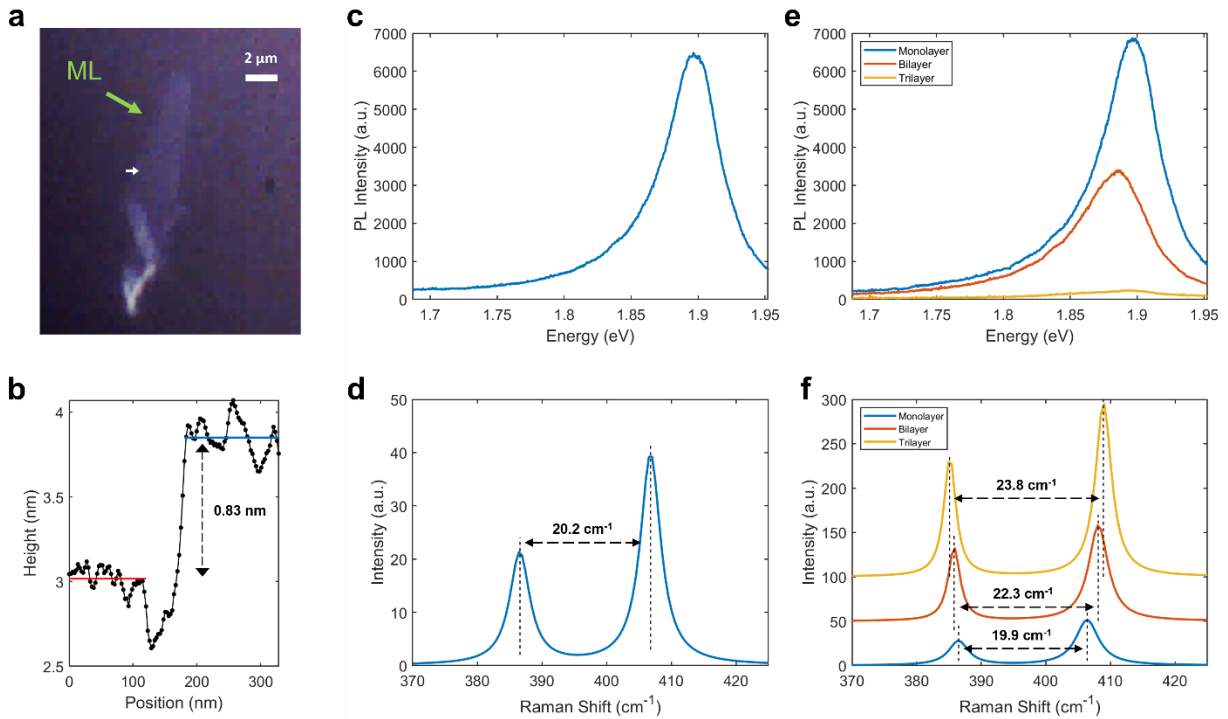
Figure S1. (a) An optical image of the exfoliated MoS_2 flake depicted in Figures 4 and 5 of the main text before transfer from PDMS to the final Si substrate, with a monolayer region highlighted by the green arrow. Scale bar: 2 μm. (b) depicts the AFM height profile of the step shown by the white arrow in (a), measured after the sample had been transferred to Si. The red and blue lines represent the average height of the Si and MoS_2 respectively, with a difference of 0.83 nm. The same monolayer was characterized via photoluminescence (c) and Raman spectroscopy (d) using a 532 nm laser. (e) and (f) show the photoluminescence and Raman spectra, respectively, for

1 monolayer (blue), bilayer (red), and trilayer (yellow) areas of another flake on the same sample of
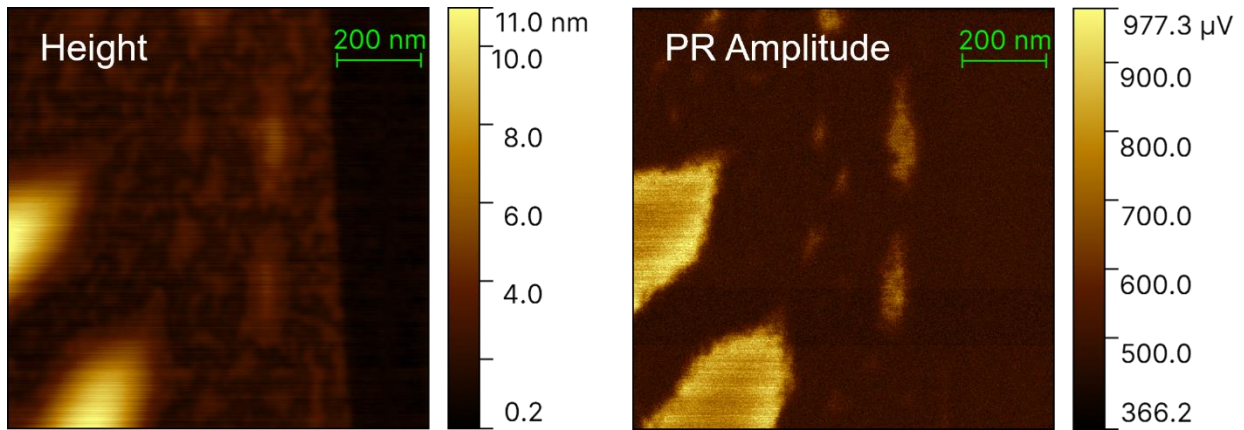
2 exfoliated MoS_2.

3

4 ***Supporting Note 2****: Classification of nanobubbles by diameter*

5   PFM results for a sample with only small nanobubbles can be seen in Figure S2, while

6 Figure S3 presents an example of a monolayer containing both small and large bubbles. Note that

7 in the latter sample there is not an even distribution of bubbles spanning the full range of sizes.

8 The majority of bubbles possess diameters less than 100 nm, while only 2-3 might be called

9 "intermediate" with diameters around 100 nm. The two biggest bubbles have diameters several

10 times those of the next smallest ones and would therefore be placed in our category of "large

11 bubbles". Figure S3 shows that the characteristic halo pattern can be observed in the piezoresponse

12 of these two large nanobubbles but not in their smaller counterparts.
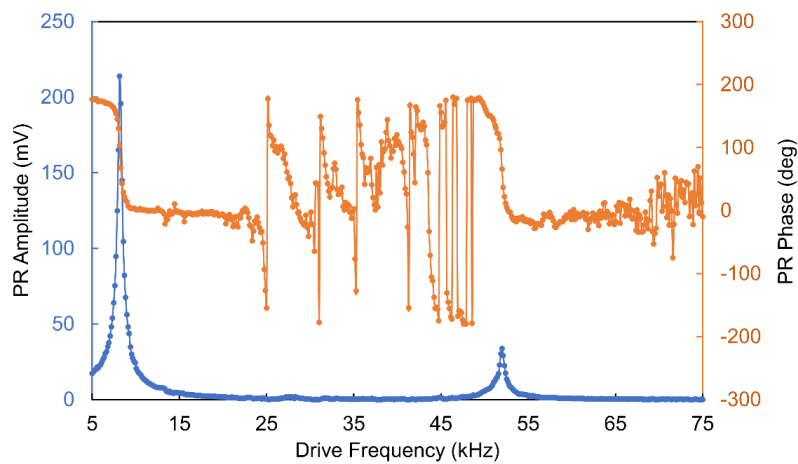

13 ☐ Mask
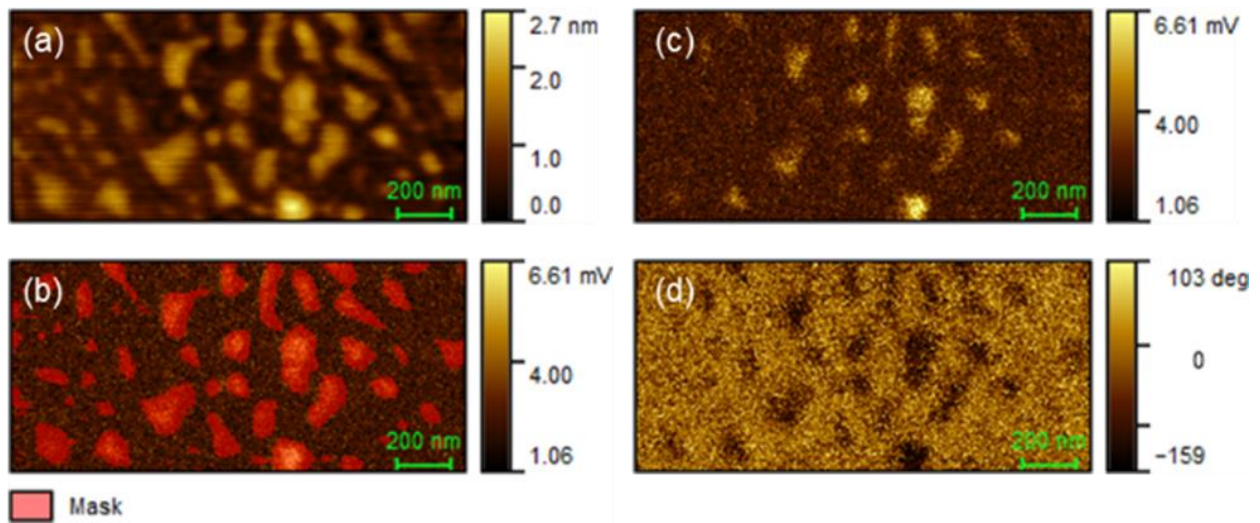
14 **Figure S2.** PFM (a) topography, (b) topography with bubbles masked, (c) amplitude and (d) phase

15 of a sample of monolayer MoS_2 on a substrate of n^{++} Si.

Figure S3. PFM height and piezoresponse amplitude of an MoS$_2$ monolayer region exhibiting both small and large nanobubbles.

Figure S4. The piezoresponse amplitude (blue) and phase (orange) vs. drive frequency on a sample of exfoliated MoS$_2$ on n^{++} Si measured with a Bruker SCM-PIC-v2 tip. PFM measurements in the main text were performed at 60 kHz drive voltage frequency where background noise in both the PR amplitude and phase signals is minimized, and the response is relatively independent of frequency.

1   ***Supporting Note 3***: *Estimation of voltage drop within MoS₂ as a function of bubble contents*

2   When the probe tip is positioned above flat regions of the sample, the bias applied between the

3   tip and substrate drops across the MoS₂ monolayer and the native oxide on the Si surface. For the

4   nanobubbles, however, the bubble's contents form an additional dielectric layer. If we apply a

5   simple planar capacitance model and assume as our boundary condition that the electric flux

6   density is equal on either side of each material junction, we obtain

7
$$\epsilon_{MoS_2}\frac{V_{MoS_2}}{t_{MoS_2}} = \epsilon_{SiO_2}\frac{V_{SiO_2}}{t_{SiO_2}} = \epsilon_{bubble}\frac{V_{bubble}}{t_{bubble}}$$

8   (S1)

9   where ϵ_m and t_m are the permittivity and thickness of material m, respectively, and V_m is the voltage

10   dropped across that material, when the index m is substituted for the MoS₂ monolayer, the SiO₂

11   native oxide on the substrate, and the bubble contents respectively. We can further state that

12
$$V_{MoS_2} + V_{SiO_2} + V_{bubble} = V_d$$

13   (S2).

14   The relative permittivity values used are 4.0, 3.9, 80, 2.4, and 1 for MoS₂, SiO₂, water,

15   hydrocarbons, and air respectively. The monolayer thickness is 0.65 nm, and the SiO₂ native oxide

16   thickness is approximated as 2 nm. The thickness of the bubble contents is determined at each

17   point as the difference between the measured AFM height and the minimum height of the flat

18   monolayer.

19   From eqs S1 and S2, we can estimate the portion of the voltage dropped across the MoS₂ layer

20   as a function of the bubble's contents and height at any given point in the scan.[4] Substituting V_{MoS2}

21   in place of the drive voltage in eq 3 of the main text alters the magnitude and shape of the effective

22   piezoelectric coefficient profile. The corrected spatial distributions of d^{eff}_{33} for the most likely

23   bubble contents are presented in Figure S5.
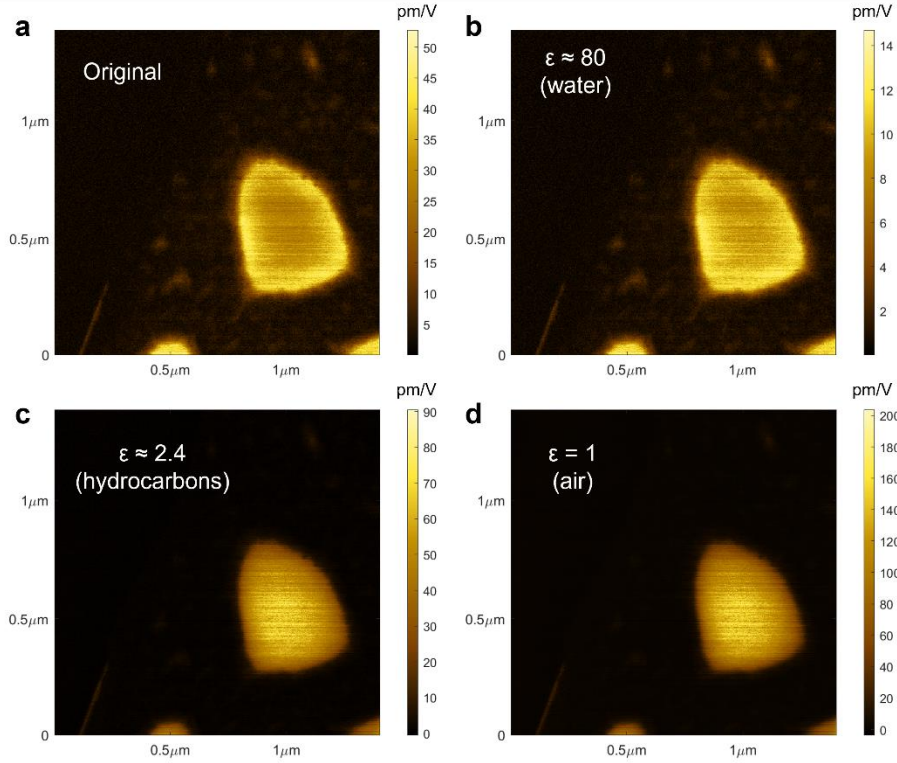
Figure S5. Effective piezoelectric coefficient d^{eff}_{33} measured via PFM of the large nanobubble in an MoS$_2$ monolayer on n^{++} Si shown in Figures 4 and 5 of the main text. The original d^{eff}_{33} calculated according to eq 3 is shown in (a). Adjusted values of V_{MoS2} calculated from eqs S1 and S2 were substituted for V_d in eq 3 to determine d^{eff}_{33} for scenarios in which various substances comprise the bubble contents. The adjusted d^{eff}_{33} is shown for the cases of the bubble containing (b) water, (c) hydrocarbons, and (d) air.

1
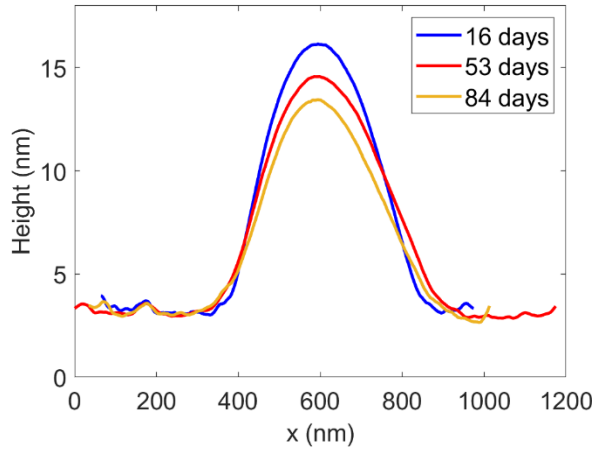
Figure S6. AFM topography linecut of the MoS$_2$ monolayer nanobubble in Figure S5 at various

times post-fabrication. Other than a small decrease in total height, the bubble is stable over

several months, indicating that the contents are primarily water.

Supporting Note 4: *Calculating strain in MoS$_2$ from its height profile*

The nanobubble strain profiles were calculated according to the method described by De

Palma et. al.[6], which is summarized as follows. Monolayer MoS$_2$ has a thickness much smaller

than the lateral dimensions of our experiment and can be mechanically modeled as a thin plate. As

a result, the stress components σ_{xz}, σ_{yz}, σ_{zz} are small compared to the other components of the stress

tensor. The resulting out of plane strain components are

$$\varepsilon_{zz} = -\upsilon(\varepsilon_{xx} + \varepsilon_{yy})/(1 - \upsilon)$$

(S3)

$$\varepsilon_{xz} = \varepsilon_{yz} = 0$$

(S4)

where v is the Poisson ratio of MoS$_2$. It should be noted from eq S3 that the out of plane strain is not zero for thin plates, but rather proportional to hydrostatic strain. In the case of MoS$_2$, $v = 0.27$[7] and $\varepsilon_{zz} = 0.74\varepsilon_{hyd}$. The components of the in-plane strain tensor for plates are related to the stress by:

$$\varepsilon_{xx} = \left(\sigma_{xx} - v\sigma_{yy}\right)/E,$$

$$\varepsilon_{yy} = \left(\sigma_{yy} - v\sigma_{xx}\right)/E,$$

$$\varepsilon_{xy} = (1 + v)\sigma_{xy}/E$$

(S5)

where E is the elastic modulus of MoS$_2$. The two-dimensional strain tensor for large transverse displacement of plates is defined by

$$\varepsilon_{\alpha\beta} = \frac{1}{2}\left(\frac{\partial u_\alpha}{\partial x_\beta} + \frac{\partial u_\beta}{\partial x_\alpha}\right) + \frac{1}{2}\frac{\partial h}{\partial x_\alpha}\frac{\partial h}{\partial x_\beta}$$

(S6)

where u is the in-plane displacement and h is the transverse displacement. The equations for equilibrium of thin plates are derived by minimizing the free energy, which has a bending and stretching component. The equations of equilibrium, termed the Föppl-Von Kármán equations, are:

$$D\nabla^4 h - t\frac{\partial}{\partial x_\beta}\left(\sigma_{\alpha\beta}\frac{\partial h}{\partial x_\alpha}\right) = P$$

(S7)

$$\frac{\partial \sigma_{\alpha\beta}}{\partial x_\beta} = 0$$

(S8)

Solving these equations can be simplified by introducing the Airy stress function, χ, defined by

$$\sigma_{xx} = \frac{\partial^2 \chi}{\partial y^2}, \qquad \sigma_{yy} = \frac{\partial^2 \chi}{\partial x^2}, \qquad \sigma_{xy} = -\frac{\partial^2 \chi}{\partial x \partial y}$$

(S9)

whereby eq S8 is automatically satisfied, reducing the number of Föppl-Von Kármán equations from 3 to 2. A new equation can be derived in terms of the stress function by substituting eqs S6 and S9 into eq S5 to obtain

$$\nabla^4 \chi + E \left\{ \frac{\partial^2 h}{\partial x^2} \frac{\partial^2 h}{\partial y^2} - \left(\frac{\partial^2 h}{\partial x \partial y} \right)^2 \right\} = 0$$

(S10)

Eqs S7 and S8 then form a complete system of equations for deflection of large plates. We can then obtain the stresses and strains by solving for χ using eq S10. In order to solve this biharmonic equation for the stress function, we treat the problem as two weakly coupled Poisson equations[8]:

$$\nabla^2 \psi = -E \left\{ \frac{\partial^2 h}{\partial x^2} \frac{\partial^2 h}{\partial y^2} - \left(\frac{\partial^2 h}{\partial x \partial y} \right)^2 \right\}$$

(S11)

$$\nabla^2 \chi = \psi$$

(S12)

1   The procedure for solving for the strain is then to first solve eq S11 using the gaussian curvature

2   from the AFM topography and use the result to solve eq S12. Assuming the flat MoS$_2$ areas away

3   from the bubble to be relatively unstrained, the boundary condition $\psi=0$ is employed outside the

4   bubble perimeter. For the additional degrees of freedom, the boundary condition $\chi=0$ is applied

5   around a circular perimeter which encloses the entire area with a large radius. The choice of

6   constant for χ on the boundary does not affect the stress/strain result, as the stress and strain are

7   derived from the second derivatives of χ. Figure S7 shows the AFM height image of a large

8   nanobubble along with the components of the strain tensor calculated using the above method.

9

10
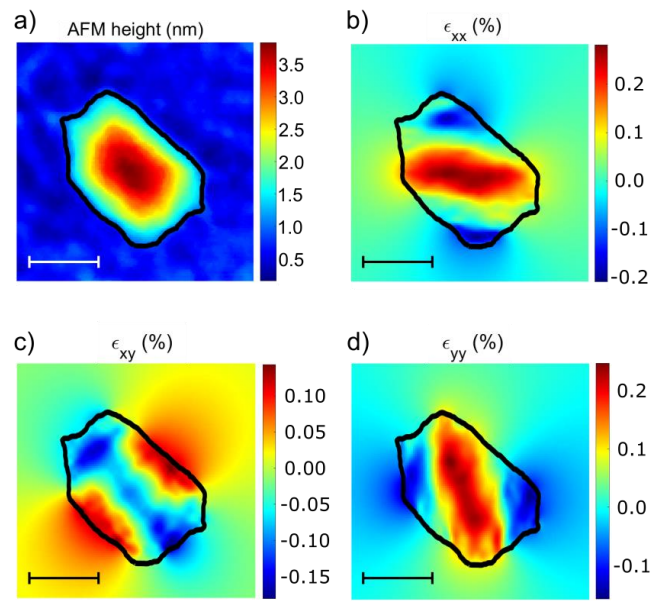
Figure S7. (a) AFM topography of a nanobubble in monolayer MoS$_2$ on Si. (b, c, d) Spatial

distribution of the components of the two-dimensional strain tensor. The scale bar represents 200

nm.

14

15

REFERENCES

(1)   Shearer, C. J.; Slattery, A. D.; Stapleton, A. J.; Shapter, J. G.; Gibson, C. T. Accurate Thickness Measurement of Graphene. *Nanotechnology* **2016**, *27* (12). https://doi.org/10.1088/0957-4484/27/12/125704.

(2)   Nemes-Incze, P.; Osváth, Z.; Kamarás, K.; Biró, L. P. Anomalies in Thickness Measurements of Graphene and Few Layer Graphite Crystals by Tapping Mode Atomic Force Microscopy. *Carbon* **2008**, *46* (11), 1435–1442. https://doi.org/10.1016/j.carbon.2008.06.022.

(3)   Munkhbayar, G.; Palleschi, S.; Perrozzi, F.; Nardone, M.; Davaasambuu, J.; Ottaviano, L. A Study of Exfoliated Molybdenum Disulfide (MoS2) Based on Raman and Photoluminescence Spectroscopy. *Solid State Phenomena* **2018**, *271*, 40–46. https://doi.org/10.4028/www.scientific.net/SSP.271.40.

(4)   Brennan, C. J.; Ghosh, R.; Koul, K.; Banerjee, S. K.; Lu, N.; Yu, E. T. Out-of-Plane Electromechanical Response of Monolayer Molybdenum Disulfide Measured by Piezoresponse Force Microscopy. *Nano. Lett.* **2017**, *17* (9), 5464–5471. https://doi.org/10.1021/ACS.NANOLETT.7B02123.

(5)   Tamulewicz, M.; Kutrowska-Girzycka, J.; Gajewski, K.; Serafińczuk, J.; Sierakowski, A.; Jadczak, J.; Bryja, L.; Gotszalk, T. P. Layer Number Dependence of the Work Function and Optical Properties of Single and Few Layers MoS2: Effect of Substrate. *Nanotechnology* **2019**, *30* (24), 245708. https://doi.org/10.1088/1361-6528/ab0caf.

(6)   De Palma, A. C.; Peng, X.; Arash, S.; Gao, F. Y.; Baldini, E.; Li, X.; Yu, E. T. Elucidating Piezoelectricity and Strain in Monolayer MoS2 at the Nanoscale Using Kelvin Probe Force Microscopy. *Nano. Lett.* **2024**, *24* (6), 1835-1842. https://doi.org/10.1021/acs.nanolett.3c03100.

(7)   Feldman, J. L. Elastic Constants of 2H-MoS2 and 2H-NbSe2 Extracted from Measured Dispersion Curves and Linear Compressibilities. *Journal of Physics and Chemistry of Solids* **1976**, *37* (12), 1141–1144.

(8)   Darlington, T. P.; Krayev, A.; Venkatesh, V.; Saxena, R.; Kysar, J. W.; Borys, N. J.; Jariwala, D.; Schuck, P. J. Facile and Quantitative Estimation of Strain in Nanobubbles with Arbitrary Symmetry in 2D Semiconductors Verified Using Hyperspectral Nano-Optical Imaging. *Journal of Chemical Physics* **2020**, *153* (2). https://doi.org/10.1063/5.0012817.